frontiers in Physics

ORIGINAL RESEARCH
published: 18 March 2020
doi: 10.3389/fphy.2020.00052

Correlation Between Bands Structure and Quantum Magneto Transport Properties in InAs/$Ga_xIn_{1-x}Sb$ Type II Superlattice for Infrared Detection

Nassima Benchtaber, Abdelhakim Nafidi, Driss Barkissy, Abderrezak Boutramine, Merieme Benaadad, Samir Melkoud, Es-Said Es-Salhi and Fatiha Chibane*

Laboratory of Condensed Matter Physics and Nanomaterials for Renewable Energy, Physics Department, Faculty of Science, Ibn Zohr University, Agadir, Morocco

We have used the envelope function formalism to investigate the bands structure of LWIR type II SL InAs ($d_1 = 2.18d_2$)/$In_{0.25}Ga_{0.75}Sb$($d_2 = 21.5$ Å). Thus, we extracted optical and transport parameters as the band gap, cut off wavelength, carriers effective mass, Fermi level and the density of state. Our results show that the higher optical cut-off wavelength can be achieved with smaller layer thicknesses. The semiconductor-semi metal transition was studied as a function of temperature. Our results permit us the interpretations of Hall and Shubnikov-de Haas effects. These results are in agreement with experimental results in literature and a guide for engineering infrared detectors.

Keywords: bands structure, quantum magneto transport, Shubnikov-de Haas effect, density of states, InAs/$Ga_xIn_{1-x}Sb$ superlattice, infrared detection

OPEN ACCESS

Edited by:
Lorenzo Pavesi,
University of Trento, Italy

Reviewed by:
Philippe Christol,
Université de Montpellier, France
Frank Rutz,
Institute for Applied Solid State Physics (FHG), Germany

****Correspondence:***
Nassima Benchtaber
nassimabenc@gmail.com

Specialty section:
This article was submitted to Optics and Photonics, a section of the journal Frontiers in Physics

Received: *02 July 2019*
Accepted: *20 February 2020*
Published: *18 March 2020*

Citation:
Benchtaber N, Nafidi A, Barkissy D, Boutramine A, Benaadad M, Melkoud S, Es-Salhi E-S and Chibane F (2020) Correlation Between Bands Structure and Quantum Magneto Transport Properties in InAs/$Ga_xIn_{1-x}Sb$ Type II Superlattice for Infrared Detection. Front. Phys. 8:52. doi: 10.3389/fphy.2020.00052

INTRODUCTION

There are a several efforts in developing infrared materials for Very Long Wavelength Infrared (VLWIR) photodetection with the optical cut-off wavelengths $\lambda_c \geq 7.5\,\mu m$ in the atmospheric window. Currently, InAs/$In_{1-x}Ga_xSb$ type-II superlattices (SLs) are still the most promising candidate. In this area, Smith and Mailhiot [1] have shown that this material system provides distinctive advantages suitable for VLWIR photodetection.

The key lies in the fact that by increasing indium composition in $In_{1-x}Ga_xSb$ layer, the corresponding lattice constant increases. As a result, the tension in the InAs layer lowers the conduction subbands (E_i) whereas the compression in the $In_{1-x}Ga_xSb$ layer raises the heavy hole subband (HH_i). Therefore, a very smaller band gap can be optimized with a reasonably thinner period which is not possible in InAs/GaSb SL [2]. The most important advantage of this SL lies in the fact that the presence of strain within this SL layers reduces the Auger recombination process and improves significantly the carrier lifetime and detectivity [3]. We note that in the previous years, a very few works were reported to verify the theoretical performance of InAs/InGaSb SLs for LWIR and VLWIR photodetection.

The applications of this technology are in military, automobile, aircraft safety, medical diagnosis, and in remote sensing systems [4].

The theory of band structure is necessary for describing the effects of external excitations on transport parameters and properties of optoelectronics devices [5]. Owing to this lack of studies, we have investigated the bands structure of presented LWIR type II SL InAs ($d_1 = 47$ Å)/$Ga_{0.75}In_{0.25}Sb$($d_2 = 21.5$ Å) with $d_1/d_2 = 2.186$ along the wave vector k_z in the growth

direction and $k_p(k_x,k_y)$ in-plane of the superlattice. We extracted useful electro-optical parameters like the optical cut-off wavelength, the effective mass of electrons and holes and their evolution with temperature. We found the point of semiconductor (SC) to Semimetal (SM) transition. We calculated the density of states without and with applied magnetic field and deduced the dimensionality and the limit of the quantification of the energy of electron gas.

THEORY AND BAND STRUCTURE

The general expression of dispersion relation of type-II SLs, within the envelope function formalism and effective mass approximation, is given by [6–9]:

$$cos\,(k_z d) = cos\,(k_1 d_1) cos\,(k_2 d_2) - \frac{1}{2}\left[\left(\xi + \frac{1}{\xi}\right) + \frac{k_p^2}{4k_1 k_2}\left(r + \frac{1}{2} - 2\right)\right] sin\,(k_1 d_1) sin\,(k_2 d_2), \quad (1)$$

In each host material, we used the six bands Kane Hamiltonian (6*6 matrix) describing the k.p interaction of Γ_6 doublet ($\left|S, m_j^s = \pm 1/2\right\rangle$ for electrons) and Γ_8 quadruplet ($\left|P, m_j^p = \pm 1/2\right\rangle$ for light holes and $\left|P, m_j^p = \pm 3/2\right\rangle$ for heavy holes]. The spin-orbit coupling is too large, compared to the hosts gaps ε_i, so the Γ_7 doublet is neglected. With the help of the Bloch condition, the continuity of the envelope functions and their derivatives at the interfaces we obtain a system with solution Equation (1). The inferior limit of the validity of this model is $d_1 < 10$ Å and $d_2 < 10$ Å as indicated by Bastard [6], Andlauer and Vog [7], Masur et al. [8]. Here k_z and $k_p(k_x,k_y)$ are the wave vector in the growth direction and in-plane of the superlattice. The origin of the energy E has been chosen at the top of InAs valence band as shown in the **Figure 1**. In each host material and for a given energy, the two–band Kane model [10] gives the wave vector ($k_i^2 + k_p^2$). Therefore, the energy E of the light particles (electron and light hole) is given by:

$$\begin{cases} \frac{2}{3}P_1^2\hbar^2\left(k_1^2 + k_p^2\right) = (E - \varepsilon_1)\,E \quad for\ InAs \\ \frac{2}{3}P_2^2\hbar^2\left(k_2^2 + k_p^2\right) = (E - \varepsilon_2 - \Lambda)\,(E - \Lambda) \quad for\ InGaSb \end{cases}, (2)$$

The expression of ξ and r in the Equation (1) are:

$$\xi = \frac{k_1}{k_2}\,r \text{ and } r = \frac{E - \Lambda - \varepsilon_2}{E - \varepsilon_1}$$

From the same Equation (1), the superlattice heavy holes mini-bands can be calculated with the following relations:

$$\begin{cases} -\frac{1}{2}\frac{\hbar^2}{(m_{hh}^*)_1}\left(k_1^2 + k_p^2\right) = E \quad for\ InAs \\ -\frac{1}{2}\frac{\hbar^2}{(m_{hh}^*)_2}\left(k_2^2 + k_p^2\right) = (E - \Lambda) \quad for\ InGaSb \end{cases}, \quad (3)$$

$$\xi = \frac{k_1}{k_2}\,r \text{ and } r = \frac{(m_{hh}^*)_2}{(m_{hh}^*)_1}$$

The direct band gaps parameters ε_i (i = 1 and 2) used here, as a function of temperature, are given by the empirical expressions reported in Matossi and Stern [11] and Roth et al. [12]. P_i is the Kane matrix element.

The heavy holes effective masses of InAs and $In_{0.25}Ga_{0.75}Sb$ are, respectively $(m_{hh}^*)_1 = 0.41\ m_0$ and $(m_{hh}^*)_2 = 0.42\ m_0$, as given in Levinshtein et al. [13]. Here m_0 is the free electron mass.

In this work, we have used the valence band offset Λ of 510 meV between heavy holes sub-bands edges of InAs and $In_{0.25}Ga_{0.75}Sb$ [14]. The origin of energy is taken on the top of VB in InAs (**Figure 1**).

The computation of band structures consists of solving the general dispersion relation with the reported parameters. In the Equation (1), state energy exists if the right-hand side lies in the range −1 to 1. In other words, $-1 \leq \cos(k_z d) \leq 1$ which implies $-\pi/d \leq k_z \leq \pi/d$ in the first Brillouin zone, with $d = d_1 + d_2$ is the superlattice period. In the study of energy E as a function of wave vector in the direction of growth k_z ($k_p = 0$), the solving procedure consists of going with small steps of energy through the studied range. Then finding, for a given E, the value of k_z which is root of the dispersion relations. The same procedure is used for studying E vs. the in-plane wave vector k_p ($k_z = 0$ and $k_z = \pi/d$).

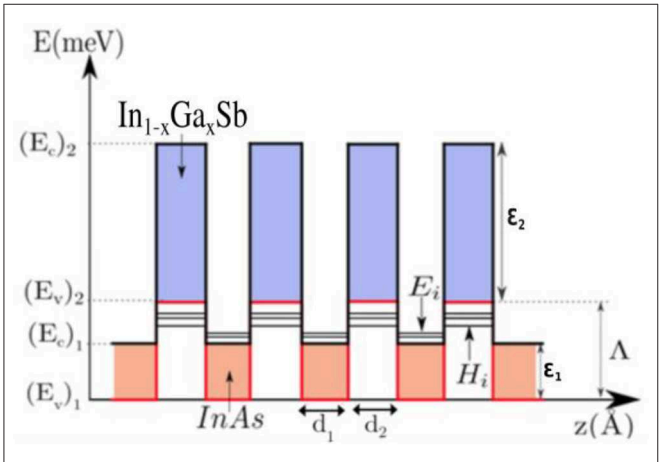

FIGURE 1 | Energy bands alignment in InAs/$In_{1-x}Ga_xSb$ SL along the growth axis z. $(E_c)_i$, $(E_v)_i$, and ϵ_i where i = 1 and 2 are conduction and valence band edges and band gap of bulks, respectively. $\Delta E_v = \wedge$ is the valence band offset.

RESULTS AND DISCUSSIONS

Bands Structures, Band Gap, Cut Off Wavelength, and Carriers Effective Mass

In the **Figure 2**, we have plotted the energy of conduction (E_i), light-hole (h_i), and heavy-hole (HH_i) subbands at the center Γ($k_z = 0$) and the limit ($k_z = \pi/d$) of the first Brillouin zone (FBZ) as a function of $d_1 = 2.18\ d_2$ at 1.2 K. These results show that when d_1 increases, the width of E_i and HH_i deceases. In

addition, we can notice that the fundamental band gap energy $E_g(\Gamma) = E_1(\Gamma)$–$HH_1(\Gamma)$ decreases when d_1 increases. Therefore, a crossover between E_1 and HH_1 takes place at the semiconductor (SC) to Semimetal (SM) transition point $T_c(d_{1c} = 115.43$ Å, $E_{1c} = HH_{1c} = 485.25$ meV).

In **Figure 3**, at a given temperature the E_g decreases when the valence band offset ∧, between the top of the heavy hole bands in the two host materials, increases. The transition SC-SM occurs when E_g goes to zero.

The evolution of the cut off wavelength $|\lambda_c|$ as a function of d_2 is shown in **Figure 4**. These results were calculated by using the expression:

$$\lambda_c(\mu m) = \frac{1240}{E_g(meV)} \quad (4)$$

The dependencies of $|\lambda_c(\Gamma)|$ on d_2 and temperature (T) are shown in **Figure 4**. The figure divides itself into two regimes: (i) For $d_2 \leq d_{2c}$: for each T, $\lambda_c(\Gamma, d_2)$ increases significantly with increasing d_2. When d_2 exceeds the critical value of d_{2c}, E_1 is confounded with HH_1 at the SC-SM transition point where $\lambda_c(\Gamma, d_{2c})$ diverges. The critical d_{2c} decreases from 53.5 Å at 1.2 K to 37 Å at 300 K. Thus, the SC-SM transition goes to lower d_1 when T increases. (ii) For $d_2 > d_{2c}$: E_1 falls completely below HH_1 and the SL shows an inverted bands structure with a SM conductivity. In this regime a reverse behavior was observed. The inset figure shows the sensitivity of E_g on T. This result shows that when T increases E_g shifts to lower energies with 0.21 meV/K. This is due to the fact that the thermal energy and electron-phonon interaction increase with T which lead to a reduction of the potential seen by electrons, leading to a reduced E_g. In the investigated temperature range, the corresponding $7.46 \leq \lambda_c(\mu m) \leq 11.94$ situates this sample in the LWIR region. The SL bands structure shown in **Figure 5** was computed at 1.2 K along k_z and k_p the growth and in-plan directions, respectively. Along k_z, the widths of E_1 and E_2, $|E_i(k_z = \pi/d) - E_i(k_z = 0)|$,

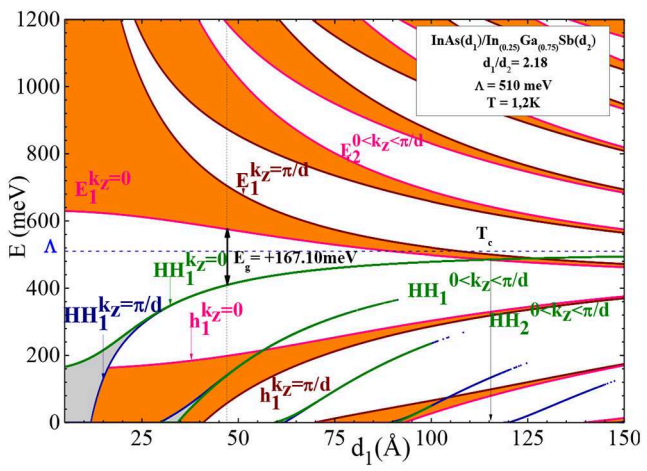

FIGURE 2 | Energy position and width of E_i, HH_i and hi subbands calculated at 1.2 K, in the FBZ as a function of d_1.

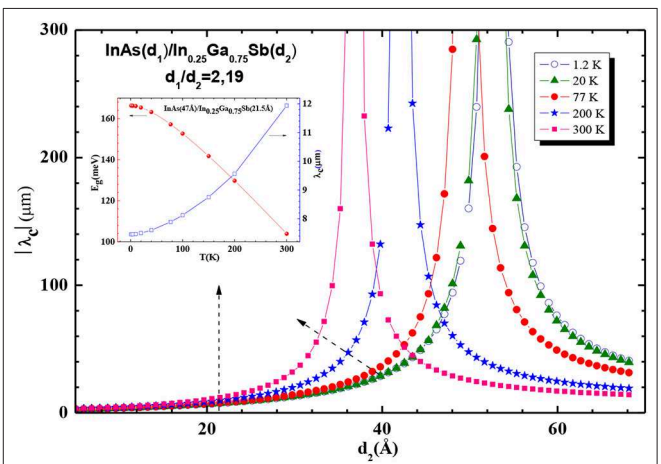

FIGURE 4 | SLs $|\lambda_c(\Gamma)|$ as a function of d_2 for various temperatures. In the insert the variation of $E_g(T)$ and $\lambda_c(T)$ with temperature in the investigated SL.

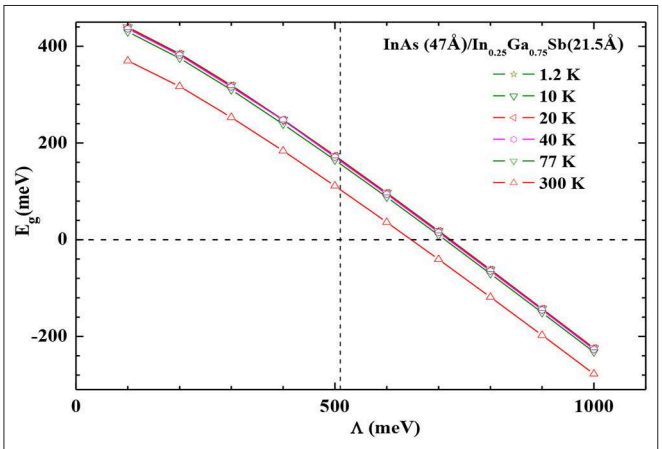

FIGURE 3 | Band gap, E_g, as a function of the valence band offset at different temperatures in the investigated superlattice. The vertical dashed line indicates our chosen value of 510 meV.

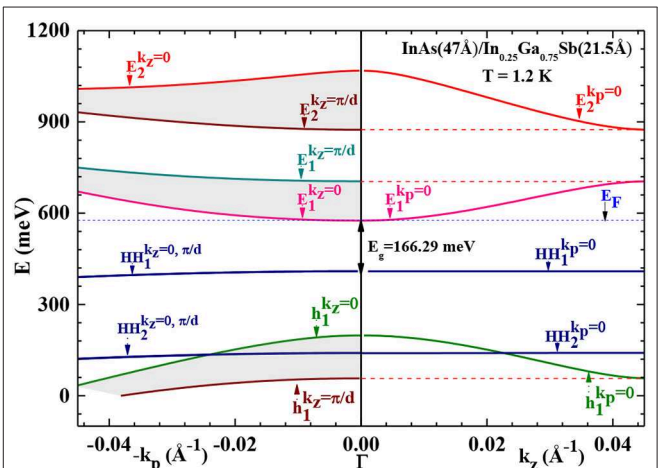

FIGURE 5 | Band structures of the investigated SL along the k_z and k_p directions.

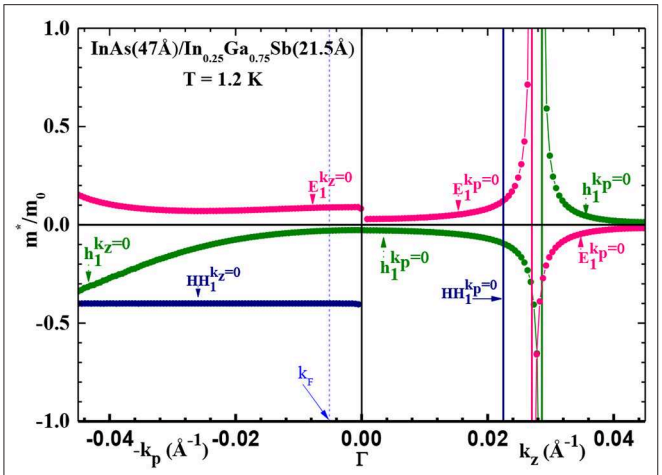

FIGURE 6 | Calculated carrier's effective mass along the growth direction and in plan of the investigated SL.

were found to be 129 and 193 meV, respectively. The presence of such dispersion indicates three dimensional like behavior of electrons which is in agreement with the reported results of Mitchel et al. [15].

The energy as a function of k_z^2 and k_p^2 at 1.2 K shows that: along k_z, the bands E_i and h_i of the light particles are non-parabolic and the heavy holes bands HH_i are parabolic; but along k_p, E_1 and HH_i are parabolic but h_1 is non-parabolic. The theoretical effective mass in general turns out to be a tensor with nine components defined as [16]:

$$\frac{1}{m_{ij}^*} = \frac{1}{\hbar^2}\frac{\partial^2 E(k)}{\partial k_i \partial k_j} \tag{5}$$

From **Figure 5** we calculated carrier's effective mass of light particles: electrons E_1, light holes h_1 and heavy holes HH_1, in the direction of growth (k_z) and in plane (k_p) of this sample. **Figure 6** shows that along k_p, $m^*_{HH1}(k_p) = -0.41\ m_0$ whereas $m^*_{E1}(k_p)$ increases from 0.092 m_0 to 0.151 m_0 and $m^*_{h1}(k_p)$ decreases from −0.026 to −0.339 m_0 at $k_p = \pi/d$. Along k_z, $m^*_{E1}(k_z)$ and $m^*_{h1}(k_z)$ diverge at inflection points $k_z = 0.0269$ Å^{-1} and $k_z = 0.103$ Å^{-1}, respectively. At these points the effective mass changes its sign, in electron and light-hole bands. The dashed vertical line indicate the $m^*_{E1}(k_p) = 0.0887\ m_0$ at the Fermi wave vector k_F. Rogalski [17] gives a larger electron effective mass $m^*/m_o \approx 0.02$–0.03 in InAs/GaInSb SLs, compared to $m^*/m_o = 0.009$ in HgCdTe alloy with the same bandgap $E_g \approx 100$ meV. These values are indicated without d_1, d_2, temperature and direction of the effective mass tensor. Our results at the center Γ of the first Brillouin zone are $m^*_{E1}(k_p) = 0.092\ m_0$, $m^*_{E1}(k_z) = 0.026\ m_0$, $m^*_{h1}(k_p) = m^*_{h1}(k_z) = -0.026\ m_0$, and $m^*_{HH1}(k_p) = -0.41\ m_0$.

Interpretations of Hall Effect, the Density of States, and the Dimensionality of Carrier's Charges

We used the carrier density n as a function of the inverse of temperature measured in Mitchel et al. [18] and Haugan et al. [19]. In order to determine the band gap with accuracy, we plotted $nT^{-3/2}$ as a function of 1,000/T. This lead to an experimental band gap of $E_g = (95 \pm 8)$ meV in the intrinsic domain, which is in agreement with our 104 meV calculated at 300 K. The observed difference of 8.87 meV is due to the reduction of the gap by strain [1] and the input parameters considered here as well as fluctuations during the growth of SL which could affect E_g. Note that Szmulowicz [20] and Szmulowicz et al. [21, 22] have studied the band structures of InAs(d_1 = 43.6 Å)/$In_{0.23}Ga_{0.77}Sb$(d_2 = 17.3 Å) with $d_1/d_2 = 2.52$ and the origin of energy taken at the bottom of the conduction band in InAs. The InAs conduction band–GaSb valence-band overlap was taken to be 140 meV. The band gap in this structure was tailored to be 120 meV. Whereas, Mitchel et al. [15] told a calculated $E_g = 66.4$ meV for this same sample. It's a contradiction and in addition the temperature of calculation of the gap was not given. From carrier density vs. inverse of temperature [18, 19], we deduced the activation energy E_a-$E_g = 0.196$ meV at low temperatures in agreement with the magnitude of thermal activation energy k_BT at 2.3 K.

We plot the measured mobility μ in Mitchel et al. [18] and Haugan et al. [19] vs. temperature in logarithmic scales. This shows that when T increases, μ decreases as $T^{-1.5}$ indicating the interaction of electrons with phonons in the intrinsic regime. This result confirms a tridimensional electron gas.

For the superlattice i^{th} mini-band, with energy width $\Delta E(i) = E(i)_{max} - E(i)_{min}$, the density of states (DOS) can be expressed as [23]:

$$\rho_{DOS}^{(i)}(E) = \begin{cases} \left(m^*/\pi^2\hbar^2\right) k_z(E) \, for \, E_{\min}^{(i)} \le E \le E_{\max}^{(i)} \\ 0 \quad otherwise \end{cases} \tag{6}$$

The generalization of Equation (6) required a sum over all mini-bands:

$$\rho_{DOS}(E) = \sum_{i=1}^{n} \rho_{DOS}^{(i)}(E) \tag{7}$$

From the dispersion curves $E(k_z)$ in **Figure 5**, we have calculated the SL density of states (DOS) of the two lowest conduction minibands E_i and the first valence subband HH_1 at 1.2 K. As seen in **Figure 7**, the DOS is quantized in term of $m^*/\pi\hbar^2 d$, with the presence of large dispersion in E_i. This shows a significant interaction between InAs wells justified by the ratio $d_1 = 2.18\ d_2$ in this sample.

At given temperature the Fermi level energy was obtained by the formula:

$$E_F = E_{E1} + \frac{\hbar^2 (k_F^i)^2}{2m_{E1}^*} \quad \text{with}$$
$$k_F^{2D} = (2\pi n)^{1/2} \quad \text{and} \quad k_F^{3D} = (3\pi^2 n)^{1/3} \tag{8}$$

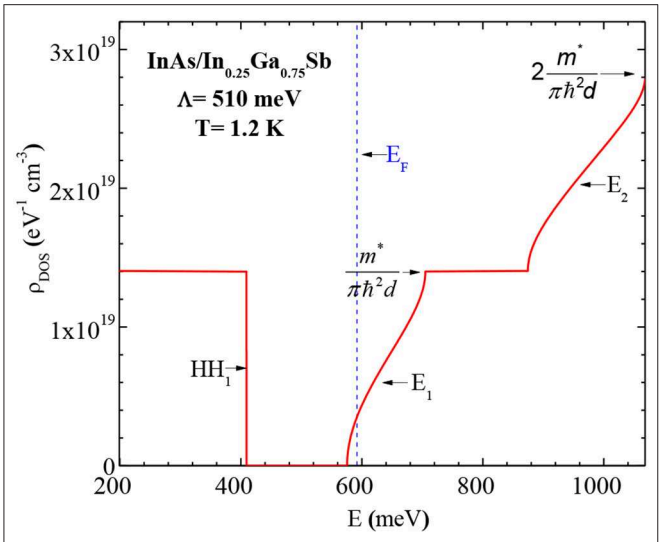

FIGURE 7 | The SL DOS of the three subbands HH1, E_1, and E_2 at 1.2 K. The vertical dashed line indicates the position of the Fermi level energy E_F.

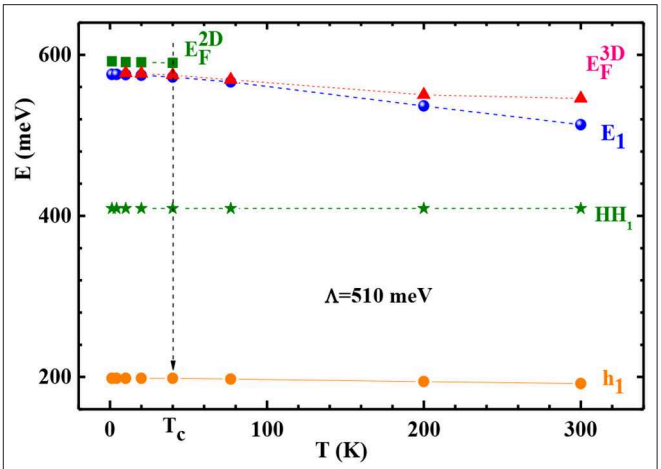

FIGURE 8 | Energy of the first conduction (E_1), valence (HH_1 and h_1) subbands, two and three dimensional Fermi level energy (E_F) at different temperatures.

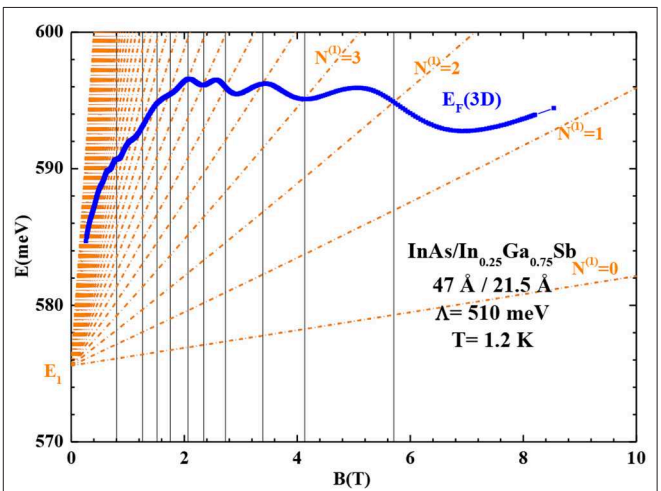

FIGURE 9 | Calculated Landau levels of E_1 as a function of the applied magnetic field in the investigated SL at 1.2 K. E_F is the Fermi level energy.

where k_F^{2D} and k_F^{3D} are the two dimensional and three dimensional Fermi wave vector, respectively and n is the measured concentration of carrier charge in the n(T) type sample [18, 19]. The effective masse of electrons at the Fermi wave vector k_F is $m^*_{E1}(k_F) = 0.0887\ m_0$ from **Figure 6**. The formula (8) permit as the determination of E_F, at the center Γ of the first Brillouin zone, where all the bands are parabolic as seen in **Figure 5**.

In **Figure 7**, the calculated Fermi level energy E_F is on the large E_1 band indicating an n type (in agreement with [18, 19]) and quasi-bidimensional (Q2D) conduction behavior. Whereas, the full first valence subband HH_1 has a very narrow band width indicating 2D-like behavior. The observation of Mitchel et al. [15] indicated a tridimensional conduction (3D).

In order to precise the dimensionality of carriers charges we plot, **Figure 8** which shows the energy bands of light (h_1), heavy (HH_1) holes, and E_1 electrons as a function of temperature. As can be seen, the band gap E_1-HH_1 decreases as the temperature increases. The Fermi level E_F(3D) decreases with E_1 when T increases. This is the behavior of a three-dimensional electron gas. For a two-dimensional electron gas the energy of Fermi level E_F(2D) is constant i.e., independent of temperature as seen on the top of **Figure 8**. One can argue that the electron gas is Q2D up to $T_c = 40$ K and 3D for $T \geq T_c$. We are witnessing a Q2D to 3D transition. In the following, we will consider that the electron gas is three-dimensional at temperature domain under consideration.

In the Mitchel et al. [18], Haugan, et al. [19], Szmulowicz [20], and Szmulowicz et al. [21, 22] the conduction bands E_1 and E_2 widths were $\Delta E_1 = E_1(k_z = \pi/d) - E_1(k_z = 0) = 136.2$ meV and $\Delta E_2 = E_2(k_z = 0) - E_2(k_z = \pi/d) = 183.3$ meV, respectively, with a separation between them $\Delta E(k_z = \pi/d) = E_2\text{-}E_1 = 232.5$ meV in the sample $InAs(d_1 = 43.6\ Å)/In_{0.23}Ga_{0.77}Sb(d_2 = 17.3\ Å)$ with $d_1/d_2 = 2.52$. The width of HH_1 was 0.01 meV along k_z. Whereas, at 1.2 K, our calculated bands structure indicated $E_g = 166.3$ meV, $\Delta E_1 = 123$ meV, $\Delta E_2 = 193$ meV, and $\Delta E(k_z = \pi/d) = 169.4$ meV. The widths of HH_1 are 0.05 meV and 20.8 meV along k_z and k_p, respectively. The band HH_1 is flat along k_z in **Figures 1**, **5** along $q = k_z$ in Szmulowicz [20] and Szmulowicz et al. [21, 22]. These values are in the same range as those given by Mitchel et al. [18], Haugan, et al. [19], Szmulowicz [20], and Szmulowicz et al. [21, 22] except for the band gap given there without temperature.

Interpretation of the Shubnikov-de Haas Effect and the Density of States With Magnetic Field

We have calculated the Fermi level in this SL by using the magnetoresistance results reported in Mitchel et al. [15].

It is well-known that the oscillations of longitudinal magnetoresistance at very low temperatures and under high

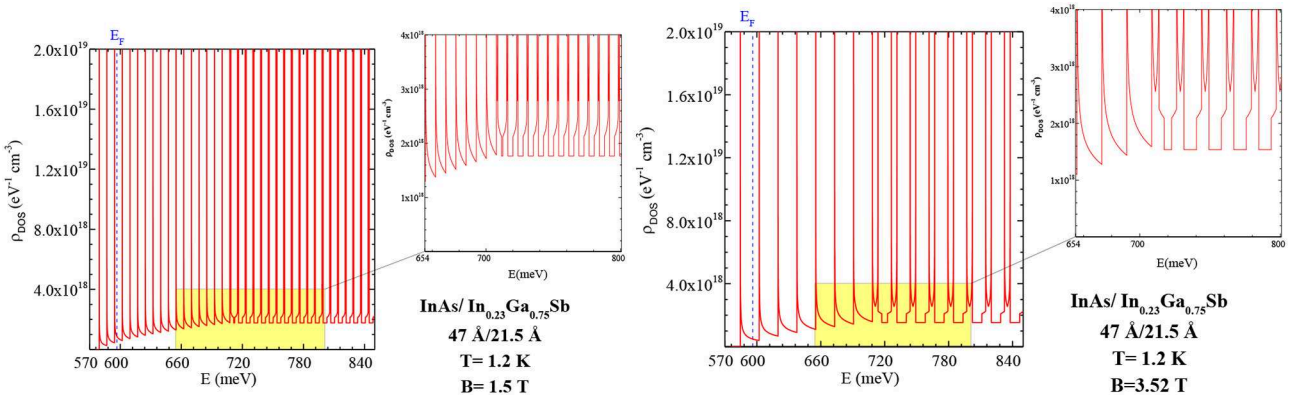

FIGURE 10 | DOS of the first conduction subband at 1.2 K in the presence of magnetic field B.

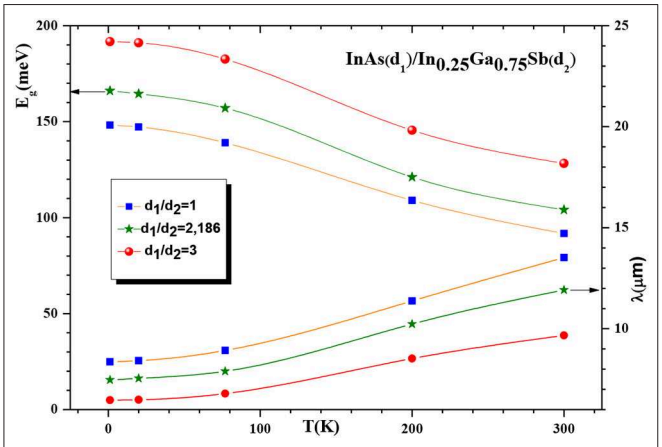

FIGURE 11 | SLs $E_g(\Gamma)$ and $|\lambda_c(\Gamma)|$ as a function of temperature for various d_1/d_2 in $InAs(d_1)/Ga_{0.75}In_{0.25}Sb(d_2)$ SL.

magnetic fields, due to the Shubnikov-de Haas effect (SdH), are periodic with respect to 1/B [24].

The inverse of the minima $1/B_m$ as a function of the entire N, Landau level index, is given by the formula:

$$\frac{1}{B_m} = \Delta\left(\frac{1}{B}\right)(N+\frac{1}{2}), \tag{9}$$

The straight line slope of (9) gives the period, $\Delta(1/B) = 1.16\ T^{-1}$. The relation between $\Delta(1/B)$ and the electron concentration n_{3D} for a 3D system is given by:

$$n_{3D} = \left(2\, e/\Delta_{1/B}\hbar\left(3\pi^2\right)^{\frac{2}{3}}\right)^{\frac{3}{2}}, \tag{10}$$

So at T = 1.2 K the SL electron density is $n_{3D} = 4.53{\cdot}10^{15}\ cm^{-3}$. The later permits us to estimate the Fermi energy by:

$$|E_F\text{-}E_1| = \left|\frac{\hbar e}{m^{\star}_{E1}.\Delta\,(1/B)}\right|, \tag{11}$$

Here, $m^*_{E1}(k_F) = 0.09\ m_0$ is the electron effective mass at the Fermi wave vector, extracted from **Figure 6**. As seen in **Figures 5**, **7**, $E_F = 576.87$ meV and the SL has an n type conductivity at 1.2 K.

In their work of InAs/InGaSb SL magnetotransport properties properties, Levinshtein et al. [13] have shown that such SL shows Shubnikov-de Haas (SdH) effect. In the **Figure 9** we show the calculated Landau levels (LL) energies of E_1 in the investigated SL. These results are obtained by transposing the quantification rule [25] of the wave vector in the plane of the SL in $E(k_p)$ plotted in **Figure 5**:

$$k_p^2 = (2N^{(i)}+1)\frac{eB}{\hbar}, \tag{12}$$

with $N^{(i)}$ the Landau index of i^{th} mini-band

$$E_F = \frac{\hbar^2}{2m^*_{E1}}\left(\frac{3\pi^2 B}{R_{xy}.e.N_{SL}.(d_1+d_2)}\right)^{2/3}, \tag{13}$$

with $N_{SL} = 73$ is the SL number of periods. The Hall resistance has been calculated with the formulate: $R_{xy}(\Omega) = h/\nu N_{SL}e^2$ and ν is the filling factor [26].

In the **Figure 9**, when the magnetic field increases, the crossover between the calculated LL energy and the Fermi level gives the same minima (at B = 5.71 T, 4.13 T, 3.40 T, 2.73 T and 2.34 T), of the Shubnikov-de Haas effect (SDH) oscillations of the transverse magneto-resistance measured by Mitchel et al. [15].

The **Figure 10** represents the computed 3D density of states (DOS) of the first conduction mini-band of the investigated SL by using the following expression [24]:

$$\rho^{3D}_{DOS}(E,B_z) = \frac{|e|\,B_z}{8\pi^2\hbar^2}\sqrt{2m^*}\sum_i\sum_{N^{(i)}=0}^{N^{(i)}_{max}}\frac{1}{\sqrt{E-\left(N^{(i)}+\frac{1}{2}\right)\hbar\omega_c}}, \tag{14}$$

As can be seen in the figure the DOS is inversely proportional to the square root of total energy and the spacing between LL increases with the applied magnetic field.

A condition for the observation of the SDH effect is that the separation $\hbar\omega_c$ ($\omega_c = eB/m^*_{E1}$ is the cyclotron pulsation) between LL must be superior to activation thermal energy k_BT. So here the magnetic field must be $B > k_B\, m^*_{E1}\, T/\hbar e = 0.9\,T$ for $T = 1.2\,K$ and $m^*_{E1} = 0.09\, m_0$. When $B < 0.9\,T$, the LLs disappear and E_1 is a continuum. This condition of quantum limit agrees well with our calculated DOS (E_1, B) in **Figure 10**.

We also calculated the transport scattering time $\tau_p = \mu_H\, m^*_{E1}/e = 0.52$ ps for Hall mobility $\mu_H = 1.02{\cdot}10^4\ cm^2/Vs$ measured at 1.2 K by Mitchel et al. [18] and Haugan et al. [19] and our $m^*_{E1} = 0.09\, m_0$. This value of τ_p can be compared to the quantum relaxation time $\tau_q = 0.5$ ps and $\tau_p = 2.34$ ps measured in AlGaN/GaN two-dimensional electron gas [27].

Fuchs et al. [28] reported for the SL1 InAs(d_1 = 34.8Å)/$Ga_{0.8}In_{0.2}Sb$(d_2 = 29Å) with $d_1/d_2 = 1.2$, $8\,\mu m \leq \lambda_c \leq 12\,\mu m$ corresponding to $103\ meV \leq E_g \leq 155\ meV$ from electroluminescence for $10\,K \leq T \leq 240\,K$. In the studied sample SL2 InAs(d_1 = 47Å)/$Ga_{0.75}In_{0.25}Sb$(d_2 = 21.5Å) with $d_1/d_2 = 2.19$, the insert of **Figure 4** shows $\lambda_c(T)$ with $7.46 \leq \lambda_c(\mu m) \leq 10.5$ and $118\ meV \leq E_g \leq 166\ meV$ for the same investigated temperature range. In particular at low temperature, E_g(77K, SL1) = 150 meV from measured dynamical impedance increases to Eg(77K, SL2) = 157 meV in agreement with the fact that E_g increases when d_1/d_2 increases at a given temperature as seen in **Figure 11**. In the SL1, an electron effective mass of 0.03 m_0 for transport perpendicular to the SL plane was used in the band-to-band tunneling model. This effective mass is in agreement with our $0.026\ m_o \leq m^*_{E1}(k_z) \leq 0.028\ m_o$ for $1.2\,K \leq T \leq 300\,K$ near the center Γ of the first Brillion zone in **Figure 6**. All these transport parameters are in the same order of transport characteristics of the investigated SL.

CONCLUSION

Using the envelope function formalism, we have investigated the electronic and optical properties of LWIR InAs(d_1 = 2.18 d_2)/$In_{0.25}Ga_{0.75}Sb$ (d_2 = 21.5 Å) type II SL. The dependencies of the band gap and the corresponding cut-off wavelength on layers' thicknesses and temperature were studied and interpreted. Our results show that a very smaller band gap can be achieved with reasonably thinner layers. The SC-SM transition was found to go to lower d_{1c} and/or d_{2c} when the temperature increases. Transport properties of this sample indicate a tridimensional conduction behavior. Whereas, the first valence subband HH_1 shows 2D-like behavior. We interpreted the Shubnikov-de Haas effect and the density of states without and as a function of magnetic field. The condition of quantum limit agrees well with our calculations. In the intrinsic regime, our results agree well with experimental observations of W. C. Mitchel et al. These results are a guide for engineering infrared detectors.

DATA AVAILABILITY STATEMENT

All datasets generated for this study are included in the article/supplementary material.

AUTHOR CONTRIBUTIONS

NB: corresponding author doing the most of the article. AN: the supervisor is correcting the article. DB: help in the band gap calculation. AB, MB, SM, E-SE-S, and FC: help in calculation of masses effective and magnetotraport. All authors have contributed to this work and approved it for publication.

REFERENCES

1. Smith DL, Mailhiot C. Theory of semiconductor superlattice electronic structure. *Rev Mod Phys.* (1990) **62**:173. doi: 10.1103/RevModPhys.62.173
2. Boutramine A, Nafidi D, Barkissy E-S, El-Frikhe H, Charifi Elanique A, Chaib H. Electronic band structure and Shubnikov-de Haas effect in two-dimensional semimetallic InAs/GaSb nanostructure superlattice. *Appl Phys A Mater Sci Process.* (2016) **122**:1. doi: 10.1007/s00339-015-9561-x
3. Grein CH, Lau WH, Harbert TL, Flatte ME. Modeling of very long infrared wavelength InAs/GaInSb strained layer superlattice detectors. *Proc. SPIE, Materials for Infrared Detectors II* Vol. 4795 (2002). doi: 10.1117/12.452265
4. Razeghi M, Minh Nguyen B. Advances in mid-infrared detection and imaging: a key issues review. *Rep Prog Phys.* (2014) **77**:082401. doi: 10.1088/0034-4885/77/8/082401
5. Esaki L. Advances in semiconductor superlattices, quantum wells and heterostructures. *J Phys Coll.* (1984) **45**:C5-3–C5-21. doi: 10.1051/jphyscol:1984501
6. Bastard G. Superlattice band structure in the envelope-function approximation. *Phys Rev B.* (1981) **24**:5693.
7. Andlauer T, Vogl P. Full-band envelope-function approach for type-II broken-gap superlattices. *Phys Rev.* (2009) **80**:035304. doi: 10.1103/PhysRevB.80.035304
8. Masur J-M, Rehm R, Schmitz J, Kirste L, Walther M. Infrared physics & technology. *Science.* (2013) **61**:129–33. doi: 10.1016/j.infrared.2013.07.014
9. Barkissy D, Nafidi A, Boutramine A, Benchtaber N, Khalal A, El Gouti T. Electronic transport and band structures of GaAs/AlAs nanostructures superlattices for near-infrared detection. *Appl Phys A.* (2017) **123**:61. doi: 10.1007/s00339-016-0629-z
10. Kane EO. Band structure of indium antimonide. *J Phys Chem Solids.* (1957) **1**:249–61. doi: 10.1016/0022-3697(57)90013-6
11. Matossi F, Stern F. Temperature dependence of optical absorption in p-type indium arsenide. *Phys Rev.* (1958) **111**:472. doi: 10.1103/PhysRev.111.472
12. Roth AP, Keeler WJ, Fortin E. Photovoltaic effect and temperature dependence of the energy gap in the In1–x GaxSb alloy system. *Can Phys J.* (1980) **58**:560. doi: 10.1139/p80-079
13. Levinshtein M, Rumyantsev S, Shur M. (Eds.). *Handbook series on semiconductor parameters. Vol. 1* Singapore: World Scientific Pub. Co. (1996). doi: 10.1142/2046-vol1
14. Gualtieri GJ, Schwartz GP, Nuzzo RG, Malik RJ, Walker JF. Determination of the (100) InAs/GaSb heterojunction valence band discontinuity by Xray photoemission core level spectroscopy. *J Appl Phys.* (1987) **61**:5337. doi: 10.1063/1.338270
15. Mitchel WC, Elhamri S, Haugan HJ, Brown GJ, Mou S, Szmulowicz F. Shubnikov–de Haas Effect in InGaSb/InAs superlattices. *J Appl Phys.* (2017) **122**:185106. doi: 10.1063/1.5010293
16. Kittel C. *Introduction to Solid State Physics, 8th Edn.* New York, NY: John Wiley & Sons. (2004). Available online at: https://www.wiley.com/en-us/9780471415268
17. Rogalski A. *Infrared Detectors, 2nd Edn.* Boca Raton, FL: CRC Press, Taylor and Francis Group. (2010). doi: 10.1201/b10319
18. Mitchel WC, Elhamri S, Haugan HJ, Brown GJ, Mou S, Szmulowicz F. Multicarrier transport in InGaSb/InAs superlattice

structures. *J Appl Phys.* (2016) 120:175701. doi: 10.1063/1.4966136
19. Haugan HJ, Ullrich B, Elhamri S, Szmulowicz F, Brown GJ, Tung LC, et al. Magneto-optics of InAs/GaSb superlattices. *J Appl Phys.* (2010) **107**:083112. doi: 10.1063/1.3391976
20. Szmulowicz F. Numerically stable secular equation for superlattices via transfer-matrix formalism and application to InAs/$In_{0.23}Ga_{0.77}Sb$ and InAs/$In_{0.3}Ga_{0.7}Sb$/GaSb superlattices. *Phys Rev B.* (1998) 57:9081.
21. Szmulowicz F, Elhamri S, Haugan HJ, Brown GJ, Mitchel WC. Carrier mobility as a function of carrier density in type-II InAs/GaSb superlattices. *J Appl Phys.* (2009) **105**:119901. doi: 10.1063/1.3137201
22. Szmulowicz F, Haugan HJ, Elhamri S, Brown GJ. Calculation of vertical and horizontal mobilities in InAs/GaSb superlattices. *Phys Rev B.* (2011) **84**:155307. doi: 10.1103/PhysRevB.84.155307
23. Cho H-S. Density of states of quasi-two, -one, and -zero dimensional superlattices. *J Vac Sci Technol B Microelectron Nano Struct.* (1989) **7**:1363. doi: 10.1116/1.584539
24. Seeger K. *Semiconductor Physics: An introduction, 9th Edn*. Berlin; Heidelberg: Springer. (2004). p. 296–303. doi: 10.1007/978-3-662-09855-4
25. Bastard G. Theoretical investigations of superlattice band structure in the envelope-function approximation. *Phys Rev B.* (1982) **25**:7584. doi: 10.1103/PhysRevB.25.7584
26. Dresselhaus MS. *Solid State Physics, Part III, Magnetic Properties of* Solids (2018). p. 75–79. Available online at: http://web.mit.edu/6.732/www/6.732-pt3.pdf
27. Saxler A, Debray P, Perrin R, Elhamri S, Mitchel W, Elsass CR, et al. Electrical transport of an AlGaN/GaN two-dimensional electron gas. *MRS Int J Nitride Semiconductor Res.* (2000) **5**:619–25. doi: 10.1557/S1092578300004841
28. Fuchs F, Weimer U, Pletschen W, Schmitz J, Ahlswede E, Walther M, et al. High performance InAs/Ga1-xInxSbInAs/Ga1-xInxSb superlattice infrared photodiodes. *Appl Phys Lett.* (1997) **71**:3251. doi: 10.1063/1.120551

Conflict of Interest: The authors declare that the research was conducted in the absence of any commercial or financial relationships that could be construed as a potential conflict of interest.